Research Square

Preprints are preliminary reports that have not undergone peer review.
They should not be considered conclusive, used to inform clinical practice,
or referenced by the media as validated information.

Future projections of Climate Hazards in Urban and Rural Areas for European Cities Using Euro-CORDEX ensemble

Natalia Zazulie
nzazulie@ictp.it

The Abdus Salam International Centre for Theoretical Physics (ICTP)

Rita Nogherotto
The Institute of Atmospheric Sciences and Climate (CNR-ISAC)

Erika Coppola
The Abdus Salam International Centre for Theoretical Physics (ICTP)

Javier Diez-Sierra
Instituto de Física de Cantabria (IFCA), CSIC-Universidad de Cantabria

Francesca Raffaele
National Institute of Oceanography and Experimental Geophysics

Graziano Giuliani
The Abdus Salam International Centre for Theoretical Physics (ICTP)

Stephen Outten
Nansen Environmental and Remote Sensing Center

Article

Keywords:

Posted Date: February 24th, 2026

DOI: https://doi.org/10.21203/rs.3.rs-8368518/v1

License: This work is licensed under a Creative Commons Attribution 4.0 International License. Read Full License

Additional Declarations: No competing interests reported.

Abstract

Climate change is intensifying the frequency and severity of environmental hazards, with distinct impacts in urban and rural areas. Cities can experience amplified risks due to the urban heat island effect and increased exposure to extremes. We analyze climate extreme indices using Euro-CORDEX regional climate models that include urban representations, focusing on 40 cities and their surrounding rural areas. Our findings highlight that city-scale hazards intensify with warming across the domain, while precipitation responses are strongly regional. Mediterranean cities exhibit robust drying and longer dry spells, whereas central and northern European cities experience the strongest and most widespread increases in heavy-precipitation extremes. Urban–rural contrasts strengthen several hazard metrics, particularly minimum-temperature extremes, with the strongest signals found in inland cities, underscoring the need for targeted adaptation measures. Understanding how global warming impacts these hazard indices is crucial for developing climate-resilient policies and strategies tailored to both urban and rural settings.

1. Introduction

Cities represent critical hotspots of climatic change, where complex interactions between land cover changes, anthropogenic heat release, and heterogeneous urban geometry significantly modify local atmospheric conditions. In Europe, where over 75% of the population lives in urban areas [1], the interplay between urbanization and climate variability has become an issue of growing scientific, environmental and policy concern. These physical changes represent the basis for the so-called Urban Heat Island (UHI) phenomenon: the urban centers often show higher temperatures compared to their rural surroundings. Beyond that, cities affect other climatic processes like local wind conditions, humidity levels, and precipitation regimes, often enhancing convective activity. Moreover, urban populations face heightened exposure and vulnerability to climate extremes, such as heatwaves, droughts, and intense rainfall events, whose frequency and intensity are projected to increase under global climate change scenarios. Consequently, understanding the mechanisms driving urban-climate interactions is essential not only for advancing scientific knowledge but also for guiding sustainable urban planning, climate adaptation, and public health strategies [2].

Extreme weather events have increased in both frequency and intensity in recent decades as a consequence of climate change [3]. In Europe, the climate is changing rapidly, and the extreme events observed in recent years provide a glimpse of what may lie ahead under continued global warming [4]. Floods, droughts, and heatwaves have increasingly disrupted ecosystems, agriculture, infrastructure, and public health across the continent [4–6]. Managing these escalating climate risks and enhancing resilience has therefore become a central concern for decision-makers at all levels of governance, from European and national to regional and local [4,7].

Climate models are increasingly incorporating urban processes to more accurately simulate city-climate interactions. High-resolution EURO-CORDEX regional climate simulations have proven especially valuable in providing an essential framework to examine the role of urban land cover in regulating temperature, humidity, and extreme weather events at the continental scale. However, a crucial challenge persists in accurately quantifying both the spatial extent and magnitude of the urban effect in such simulations, particularly given their relatively coarse horizontal resolution for city-scale analyses (approximately 12.5 km), the heterogeneous representation of urban fraction (UF), the parametrization of surface effects and the limited quality of underlying data across different models. Most applications of RCMs to urban climate have so far focused on single cities or limited regions [8–12], where the inclusion of urban canopy models has shown an improvement in the representation of the urban heat island (e.g., Huszár et al.[13]). For instance, studies over Central Europe and France demonstrated that explicit canopy parameterizations capture nocturnal warming and diurnal cycles more realistically compared to bulk schemes [13,14]. However, only a few recent efforts have extended such analyses to the continental or even global scale, notably Langednijk et al. [15] and Diez-Sierra et al. [16], who applied urban representations consistently across the CORDEX-CORE ensemble (at 25 km resolution) to assess urban climate change signals in a multi-city framework.

While convection-permitting (CP) simulations operating at kilometer-scale resolution can resolve urban morphology and local processes with far greater detail—thereby improving the representation of boundary-layer dynamics, extreme temperature events, and fine-scale UHI patterns [9,11,17,18] — their application remains constrained to individual cities or limited regions due to computational demands. As a result, CP-based projections offer valuable process-level insights but lack the spatial coverage and ensemble diversity needed for continental-scale assessments. In contrast, the EURO-CORDEX at 12 km resolution provides a uniquely comprehensive framework: it covers the full range of global warming levels with continuous, multi-decadal simulations produced by multiple RCMs downscaling multiple GCMs, yielding a multi-member ensemble suitable for robust multi-city and pan-European analyses. Despite its coarser resolution and simplified urban representation, this ensemble offers the essential advantage of geographical completeness at continental scale and statistical robustness, enabling a systematic characterization of urban climate signals across Europe under future scenarios.

Hazard indices serve as critical tools to quantify and compare risks, providing insight into how different areas respond to climate stressors. Schwingshackl et al. [19] analysed the EURO-CORDEX ensemble for 36 major European cities using three metrics: yearly maximum temperature, number of days with temperatures exceeding 30°C, and daily Heat Wave Magnitude Index. They found that ambient heat is projected to increase across all cities at 3°C global warming, with particularly strong increases in southern Europe, though the magnitude and spatial patterns of projected heat depend strongly on the chosen metric. Similarly, analyses based on the Universal Thermal Climate Index (UTCI) highlight that thermal stress patterns across Europe are shaped not only by large-scale warming but also by local geographic and urban factors. Northern European coastal cities have experienced reduced cold stress due to maritime moderation, while inland Mediterranean cities exhibit higher summer heat stress compared to coastal counterparts in the same subregion. In contrast, densely built cities with limited vegetation, such as Milan, are expected to face amplified summertime thermal stress, illustrating the combined effects of regional climate change and urban heat island intensification on human thermal comfort [20].

In this paper, we assess the climate signal across a tailored set of 40 European and Northern African cities through a systematic analysis of EURO-CORDEX simulations. The objective is to characterize how these regional climate models capture the climatic signature of urban areas and to evaluate the robustness of the simulated urban effects across Europe. This kind of analysis is needed not only for improving the fidelity of urban climate projections, but also for guiding adaptation strategies tailored to city-specific climate risks under future warming scenarios.

2. Results

2.1. Urban Heat Island of maximum and minimum temperature

2.1.1. Evaluation

The evaluation runs driven by ERA-Interim provide valuable insights into the ability of the models to represent the UHI signal for both maximum and minimum temperatures. For this analysis we use six RCMs, since the evaluation output from the model UHOH-WRF361H was unavailable when the study was conducted. UHI intensity is calculated as the difference between the daily (minimun or maximum) temperature of urban and rural grid points. Figures 1 and 2 show the annual cycle of UHI (tasmax and tasmin, respectively) compared against observations for a subset of 12 cities with sufficient data coverage. Not all models are available in all cities due the 40% minimum urban-fraction threshold (see section 4.2) used to select urban grid cells in each model. For tasmax (Fig. 1), most RCMs simulate a modest UHI intensity, generally below 2°C across the year, consistent with observations in most of the cities. The REMO2015 model stands out for producing a pronounced annual cycle, with peak values during summer months across nearly all cities, except in the NEU coastal cities (Copenhagen and Stockholm), where the signal is much weaker. This feature in REMO's performance was also shown in Langendijk et al. [15] in several cities around the globe and at a lower resolution. In Athens, observations reveal a distinct minimum in summer UHI, opposite to REMO's strong summer maximum. In Glasgow, all models show weaker UHI intensity throughout the year, although they capture the seasonal behaviour. Overall, in most of the cities the observations lay in the range of the represented UHI annual cycle by the RCMs.

For tasmin (Fig. 2), observations exhibit a stronger and more persistent UHI signal than for tasmax, with values exceeding 2–3°C in several cities throughout the year. The RCMs generally show a large inter-model variability, with REMO, RACMO and ALADIN mostly underestimating the observed UHI across the year, as opposed to RegCM, WRF381P and HadREM which tend to overestimate the tasmin annual evolution in around half of the cities. WRF381P, in particular, shows a strong annual cycle, with an overestimation of summer maxima in nearly all cities, diverging from observations. This could be partly related to the WRF model's use of a binary urban fraction (0% or 100%), which can accentuate the contrast between urban and rural grid cells and thereby amplify the simulated UHI signal. For the largest cities of London and Paris, both RegCM and HadREM3 show a good agreement with observations throughout the year. REMO shows a flattening in the annual cycle of tasmin with respect to tasmax (Fig. 1). ALADIN and RACMO show in general a large underestimation of the UHI effect, except for the cities of Hamburg, Warsaw and Copenhagen where they better align with observations than the rest of the RCMs.

The evaluation runs demonstrate that while models can capture the presence of UHI to some extent, they often struggle with its magnitude of the UHI and amplitude of the seasonal cycle. Differences between tasmax and tasmin UHI are consistently found in both observations and models, with nocturnal UHI being more intense and persistent. The RegCM model, which includes a UCM urban scheme (see Table 1), shows more intense UHI values for tasmin than most of the bulk-based models, due to the UCM scheme's ability to retain heat during the night [21]. The opposite occurs for tasmax, where the slab-based models tend to reach higher temperatures during the day in most cases.

2.1.2. Projections

In this section, we analyze future projections of mean summer UHI using the RCP8.5 scenario simulations. Figure 3 summarizes the projected tasmax UHI for each city at each of the five GWLs. For the NEU region, coastal cities (blue tones) show smaller UHI intensities, in some cases even negative, and either no change or a slight decrease with increasing GWLs, except in Copenhagen. In contrast, inland cities exhibit positive values, with London and Glasgow reaching medians around 1°C, although not much difference across GWL is evident in most of the cities except for the GWL 4 with London showing a small decrease. In WCE and EEU, where most cities are inland, the behavior is broadly similar to NEU inland sites, with UHI medians typically between 0.5 and 1°C. Moscow is an exception, showing a systematic decrease in UHI intensity with higher GWLs. In the MED region, inland cities and most coastal cities present positive UHI values, with Istanbul, Naples, Rome and Sofia showing the largest intensities of 1°C or more. Ankara stands out with a wide inter-model spread and even decreases in UHI at higher GWLs. By contrast, the coastal Northern African cities of Tunis and Algiers show small negative median values, indicating a possible suppression of the UHI effect under future warming. The negative tasmax UHI in these cities is consistent with the urban cool island (or "urban oasis") effect previously documented in hot desert environments, where the abundance of vegetation and urban albedo lead to daytime cooling relative to the surrounding bare landscape [22]. Overall, MED cities display strong spatial contrasts, highlighting the influence of local geography on diurnal UHI intensity and its future projections.

Figure 4 shows the same analysis for tasmin. Compared to tasmax, the UHI intensity is systematically larger and always positive, with inter-model spread considerably wider. In the NEU region, median UHI values are generally smaller than in other regions, typically around 1–1.5°C, except for Riga that shows higher intensities approaching 2°C. In WCE and EEU, the UHI effect ranges from 0.5 and 1.0°C of median for most cities with some cities with medians exceeding 2°C and in some cases approaching 3°C, as in Zagreb, along with substantial spread across models. There is no clear behavior toward increasing or decreasing mean summer tasmin UHI with higher GWLs — median values remain relatively stable across warming levels, with the main feature being the persistent and strong night-time UHI effect.

2.2. Hazards changes at GWLs for cities

Understanding how climate hazards intensify with rising global temperatures is essential for anticipating future risks in urban environments. To assess how climate hazards evolve with increasing global warming, we examined the projected changes in the selected extreme indices for all the grid points classified as urban, where the selected cities are located, at different Global Warming Levels (GWLs). Cities are defined as areas with an urban fraction greater than 40%, as described in Section 4.2 (“City/rural outlines”). Figure 5 presents heat maps of the change relative to the reference period (1995–2014) for each city and GWL, across a set of temperature-based indices. Each cell shows the absolute change for one index, city, and GWL, while asterisks mark statistically significant differences at the 95% confidence level according to the Student’s T-test. The figure reveals a consistent and robust temperature hazard increase across all European cities and regions, with statistically significant increases in most of the temperature-based indices as GWLs rise. Hot day indices (TX25, TX30, TX35, TX90p) exhibit strong and nearly ubiquitous increases of total number of days or day/year, particularly in the MED and WCE regions, where changes are showing a one month increase for higher GWLs. Warm night indices (TN20, TN25, TN90p) also show large relative increases across all regions, reflecting the intensification of nocturnal heat stress in urban areas. In contrast, cold-related indices such as frost days (FD) show sharp decreases, consistent with the disappearance of cold extremes under warming conditions [3,23,24] especially in NEU and EEU cities. The density of asterisks state that most of these changes are significant at the 95% confidence level, indicating a robust signal across the ensemble. The figure highlights a clear and regionally coherent increase in heat-related hazards and a decline in cold extremes with progressive warming, showing the heightened risks of urban heat stress in European and NorthAfrican cities under higher global warming levels.

Analogous to the previous figure on temperature extremes, Fig. 6 presents the change relative to the reference period (1995–2014) for a set of impact-oriented indices, specifically the Heat Index thresholds (HI41, HI32) and degree-day indicators (coolDD, heatDD), expressed as percentage of change, across European cities and GWLs. The results reveal a widespread and statistically significant intensification of heat stress conditions, with HI41 and HI32 showing sharp increases in frequency, particularly over MED and WCE cities, where changes often exceed 50 days per year at higher GWLs. Cooling degree days (coolDD) also rise consistently across regions, indicating a substantial growth in cooling energy demand under warmer climates. In contrast, heating degree days (heatDD) display robust decreases, most pronounced in NEU and EEU cities, consistent with reduced energy demand for heating. The prevalence of statistically significant changes underlines the robustness of these responses. This figure underscores strongly relevant information for the society by showing warming impacts in urban environments that point to increasing health risks from heat and shifting patterns in energy consumption.

Figure 7 presents the percentage change relative to the reference period (1995–2014) for precipitation-based indices (NDD, CDD, CWD, RX1DAY, R99p) across the selected cities and GWLs. The spatial patterns reveal regionally contrasting responses, with the MED cities standing out for a pronounced drying signal. In this region, both the number of dry days (NDD) and consecutive dry days (CDD) increase significantly with warming, while consecutive wet days (CWD) tend to decrease. Together, these changes indicate a clear shift toward more persistent drought conditions as warming intensifies. At the same time, the indices of extreme precipitation, RX1DAY and R99p, reveal strong significant increases across most of MED cities, except for the most western cities of Lisbon and Madrid. This suggests that while average wet spells become shorter, single-event extremes intensify. This dual signal of drying trends alongside more severe extreme rainfall events underscores the growing challenges for water management and flood risk in southern European urban areas. In contrast, cities in NEU, EEU and WCE display weaker or more heterogeneous changes in both dry-day and wet-day metrics (NDD, CDD, CWD), while showing clear and widespread increases in the intensity (RX1DAY) and frequency (R99p) of extreme precipitation events across all warming levels. Overall, the emerging pattern suggests that, whereas the Mediterranean experiences a dual signal of drying and intensifying extremes, the rest of Europe is projected to face a pronounced strengthening of heavy precipitation events. These differences highlight the strong regional dependence of hydrological responses to global warming and underscore the need for geographically differentiated adaptation strategies within Europe’s urban areas.

2.3. Urban Heat Island of Hazard Indices

In this section, we present an analysis of the projected UHI for the selected hazard indices. Figure 8 shows the projected UHI of threshold-based indices of tasmax and tasmin, using region-specific thresholds that are most appropriate for each case. This analysis reinforces the finding that the UHI is more evident in tasmin, with larger values across all regions for tasmin-based indices. In the NEU region, almost all cities show an increase in UHI, except for Glasgow and Oslo, where UHI effects are either negligible or non-existent. In WCE, the city of Odesa stands out with the largest UHI effect in TN25, projected to further increase, while for TX35 it shows the largest inter-model spread. The remaining cities in WCE and EEU exhibit positive UHI for both indices with increased signal in the projections. In the MED region, the UHI effect is stronger compared to other regions. The tasmax-based indices show a mixed signal in this region. In coastal cities (Algiers, Tunis, Marseille, Lisbon, and Tunis), negative UHI values in TX35 are registered and projected to persist. In contrast, inland cities show positive and increasing UHI with higher GWLs. For TN25, the behavior is more uniform across MED cities, with widespread increases in UHI, however with a larger inter-model spread as a measure of the uncertainty in future projections. To further illustrate the differences between coastal and inland cities in the Mediterranean region, Fig. 9 compares an inland city (Madrid) with a coastal city (Marseille) and allows us to make additional considerations on the choice of thresholds. The figure shows the projected values for urban grid points and their corresponding countryside for two different thresholds (TX30 and TX35). For the city of Marseille, both indices increase with rising temperatures, as expected. However, due to the nature of threshold-based indices, there is a natural upper limit close to the total number of summer days. As a result, the TX30 index reaches a maximum of about 75 days per year (median) for both the city and the countryside. This limit is dictated by the climatological characteristics of the region, meaning that further warming has a diminishing effect on the number of hot days above this threshold. In contrast, TX35 starts from lower values at lower GWLs and increases more rapidly in the countryside, resulting in a reduced or even negative UHI signal for this coastal city. This pattern highlights a key difference between urban and rural areas: while Marseille's coastal location moderates the overall UHI effect, rural areas experience more pronounced increases in extreme temperature days as warming progresses. For the inland city of Madrid, the increases in TX30 are similar in both urban and rural areas, resulting in an almost unchanged UHI in the future. In contrast, for the more extreme threshold (TX35), the lower initial values create more room for increase. As a result the urban area of Madrid experiences a steeper rate of change, leading to a projected intensification of UHI under higher GWLs. These results highlight the importance of the choice of the thresholds in shaping the interpretation of extreme indices, as different thresholds may emphasize distinct aspects of the UHI response and its evolution under warming scenarios.

Figure 10 shows an analog analysis of Fig. 8, focusing on the hazard indices NOAA Heat Index and the cooling degree day (coolDD). For the northernmost cities in NEU, the threshold of 32°C was chosen, corresponding to the threshold for extreme caution category on the Heat Index scale. In this region, a clear geographic pattern between coastal and inland cities emerges. In most coastal cities (Oslo, Riga, Saint Petersburg, Stockholm) the index shows a decrease with a large spread in the GWL 4.0 between negative and positive values. This suggests that while coastal cities may experience some moderation in heat stress, the projected warming may not lead to a significant UHI intensification. In contrast, inland cities like Birmingham, Brussels, Glasgow, Hamburg and London, show an amplification of the UHI, with increasing Heat Index values. This indicates that the combination of rising temperatures and the relative lack of cooling influences in inland areas results in more intense heat stress for urban populations. In the WCE and EEU regions, all cities exhibit a clear decrease in the Heat Index. In the MED region, the signal is again mixed, with clear increases in Madrid, Naples, and Rome, and decreases in the coastal cities of Algiers, Lisbon, Marseille and Athens. The Heat Index is constructed combining the relative humidity and maximum temperature. Figure 11 shows the relationship between those two variables in time for the period 1995–2100 separated by region. The Mediterranean and the Northern regions are divided into coastal and inland areas as these categories respond differently to changes in temperature and humidity. In general, there is a projected increase in tasmax accompanied by a decrease in relative humidity, except for the NEU inland cities. It is also clear that countryside grid points show slightly higher values of humidity than the urban ones. The combination of these different changes in the two variables, result in having different impacts on the Heat Index: in regions where increases in tasmax outpace the decrease in humidity, the heat index increases. This is evident in the NEU region, where inland cities show an amplified UHI of this index, consistent with the patterns observed in the maximum temperature vs relative humidity plot, where the relative humidity is not projected to decrease (Fig. 11, upper panel). In contrast, in WCE and EEU, the projected decrease in humidity leads to a corresponding reduction in the UHI of HI41 index, particularly under higher GWLs.

The Cooling Degree-Day (coolDD) index measures the cumulative heat load exceeding a specified temperature threshold, serving as an indicator of the potential demand for cooling energy and reflecting heat-related stress in buildings and urban environments. The projected UHI for the coolDD index is shown in Fig. 10 (right panel). The results show that nearly all cities experience an increase in this index, with urban areas showing a higher heat load compared to their surrounding rural environments. These results are in agreement with Salamanca et al. [25], who found that summertime air-conditioning energy consumption was significantly greater in urban areas than in nearby rural regions. This finding aligns with the observed UHI effect, where cities-due to higher heat retention and reduced cooling capacity- experience amplified demand for cooling, exacerbating energy consumption and heat stress.

3. Discussion and Conclusions

This paper provides an assessment of the urban imprint using a set of EURO-CORDEX-CMIP5 Regional Climate Models. This dataset is exceptional within the CORDEX framework, since the European domain is the only domain that was run at 12.5 km resolution under a coordinated multi-model experiment with more than 70 ensemble members, whereas all other CORDEX domains were run at a coarser 25 km resolution and with substantially fewer ensemble members. Over Europe, Landendjik et al [15] has shown the added value of the 12.5 km resolution over the coarser 25 km, in representing the UHI effect. Despite its unique high resolution and multi-member characteristics, the ensemble still has important limitations for urban scale studies. On one hand, many of the RCMs were run with urban scheme deactivated [26], or did not provide the description of the urban fraction of the model. The majority of the models use a bulk parametrization with the exception of RegCM, which uses a single-layer urban canopy model. On the other hand, another important aspect to accurately simulate urban processes, is that the land cover input is often outdated [15,27] and fixed for the entire simulation period, which may not be adequate to represent the urban development over time. For the next generation of EURO-CORDEX-CMIP6 [28], promisingly some RCMs will provide a dynamical evolution of land cover for the evaluation period and the single-layer urban canopy model will be adopted by multiple RCMs, beyond RegCM. Furthermore, CORDEX-CORE is expected to provide, for the first time, a coordinated global ensemble at relatively high spatial resolution (12.5 km), enabling the extension of studies of this kind to the global scale, albeit with a reduced number of ensemble members compared to the European domain.

To ensure a consistent and model-aware representation of cities across this heterogenous ensemble, we apply the urban/rural classification algorithm from Diez-Sierra et al. [16] which derives urban and countryside masks from each model's static fields (See Section 4.2). Unfortunately, the urban fraction (sfturf) data was not available for all RCMs in the EURO-CORDEX ensemble since it was not a mandatory field to publish by the modelling institutes. So for this paper, we were able to gather a total of seven RCM's urban fraction data that will be available jointly with this publication. For the upcoming CORDEX-CMIP6 experiment, this variable is classified as Tier 2, which will enable future urban climate studies with a larger ensemble. The resulting ensemble for this study encompasses seven Regional Climate Models with a total of 39 individual members, which allow a characterization of model uncertainties and provide a robust framework for assessing city-scale climate signals.

The annual cycle of UHI for maximum and minimum temperature reveals that the models tend to exhibit larger amplitude than the observations, a finding consistent with the results from Karlický et al.[29] for WRF and RegCM. As pointed out by Daniel et al. [14], evaluating the UHI in RCMs presents challenges due to the fact that observational networks locate the meteorological stations in open areas, often green parks in cities [30–32]. Recent high-density measurements in Prague have shown temperature differences exceeding 3°C between urban sites depending on local morphology, further confirming that the placement of observational stations and spatial heterogeneity can significantly flatten the observed UHI signal [33]. Similarly, observations in Hamburg reveal strong spatial variability in nocturnal UHI intensity, with a clear radial gradient pattern driven by local morphology and land-cover differences [34]. Moreover, as several studies have demonstrated, the urban heat island effect is more pronounced at night and during the summer months. The stronger nighttime UHI simulated by the RegCM model highlights the importance of incorporating detailed urban canopy schemes for capturing heat storage and release processes. In contrast, bulk-based models often overestimate daytime heating due to simplified surface parameterizations. Future projections for summer months UHI suggest no clear shift in either daytime or nighttime mean temperatures, suggesting that the models may not yet fully capture the potential shifts in UHI intensity under increasing warming levels. Moreover, these scenarios assume static city boundaries and properties (i.e., no future urban expansion or morphological transformation), which can underestimate future urban climate impacts [35,36].

Projected changes in climate hazard indices across the selected cities in the EURO-CORDEX domain reveal a clear and robust intensification of heat-related hazards with increasing global warming levels. Temperature-based indices consistently show strong increases in both daytime and nighttime extremes, particularly in the Mediterranean (MED) and Western-Central Europe (WCE) regions. Concurrently, cold-related events such as frost days markedly decline, reflecting the diminishing occurrence of cold extremes. Impact-oriented indicators further highlight the growing societal implications of these changes, with substantial increases in heat stress (HI41, HI32) and cooling energy demand (coolDD), alongside a pronounced decrease in heating requirements (heatDD). Precipitation-based indices display more regionally contrasted patterns. Mediterranean cities, in particular, show a clear drying trend characterized by longer dry spells, consistent with Spinoni et al. [37] and fewer wet days while still experiencing localized intensification of extreme rainfall events, contributing to the increasing frequency of droughts and floods in these areas. However, the most significant and spatially coherent increases in heavy-precipitation indices (RX1DAY, R99p) are projected outside the Mediterranean. Cities in Northern Europe (NEU), as well as in Eastern (EEU) and Western-Central Europe (WCE), display strong and widespread intensification of extreme rainfall across all warming levels—already evident at GWL2 and becoming significant across all cities at GWL3–4. Taken together, these results underscore a coherent and significant rise in both urban heat stress and drought hazards under higher global warming levels in southern Europe, and a pronounced strengthening of heavy-precipitation extremes across northern and central regions. These contrasts highlight the urgent need for adaptation strategies tailored to regional climate risks across Europe.

The analysis of the UHI contribution for hazard indices confirms that the urban signal remains robust across future scenarios, particularly for minimum temperature–based indices. UHIs based on tasmin-derived indices intensify consistently with increasing global warming levels across regions, whereas tasmax-based indices show greater spatial variability, with the Mediterranean standing out for its contrasting coastal and inland responses. Coastal cities show stable or diminishing of the UHI intensity for the highest temperature thresholds, reflecting the moderating effect of the sea and the saturation of the available number of summer days for which the hot-day indices are calculated, whereas inland cities exhibit clear intensification with warming. Impact-oriented metrics such as the Heat Index and cooling degree days further emphasize the amplification of urban heat stress in inland areas, driven by stronger temperature increases and limited cooling from humidity and maritime influences. Conversely, some northern and coastal cities may experience partial moderation due to declining relative humidity or threshold saturation effects. Overall, these results underscore the complex interplay between regional climate drivers, urban morphology, and local geography in shaping the future evolution of UHI-related hazards across European and Northen African cities, highlighting the need for geographically differentiated adaptation strategies.

4. Methods

4.1. EURO-CORDEX data

The EURO-CORDEX initiative [38] is the European branch of the World Climate Research Programme's (WCRP) Coordinated Regional Downscaling Experiment (CORDEX,[39]), providing high-resolution regional climate projections for Europe. It has delivered an ensemble of regional climate model (RCM) simulations at horizontal resolutions of 0.11° (approximately 12.5 km), based on the dynamical downscaling of global climate model outputs from the 5th Coupled Model Intercomparison Project (CMIP5,[40]). The simulations cover the EURO-CORDEX domain, encompassing the entire European continent and adjacent areas, and are available for multiple greenhouse gas concentration scenarios. The EURO-CORDEX ensemble represents the most recent and comprehensive high-resolution RCM data set available for climate change studies in Europe and it has been used as a reference for the regional analysis in the Intergovernmental Panel on Climate (IPCC)'s Sixth Assessment Report [41]. Its higher spatial resolution and detailed representation of physical processes offer improved simulation of regional climate features and high-impact events, such as heavy precipitation, heatwaves, and dry spells, providing added value compared to coarser-resolution global simulations [42,43].

In the present study, we use 7 RCMs from the EURO-CORDEX ensemble, gathering a total of 39 members as described in Table 1. We use the evaluation simulations (1989–2008) available for six of the seven RCMs included in our ensemble. These runs are forced by the ERA-Interim reanalysis [44] and allow us to assess model performance in reproducing the observed regional climate and urban-related features. Evaluation data from the RCM UHOH-WRF361H was not available at the time of analysis. For the climate change assessment, we further consider both historical simulations (1951–2005) and scenario integrations following the high-emission pathway RCP8.5 (2006–2100;[45]).

Each regional model represents urban areas in different ways: The RegCM4.7 was run using the Community Land Model (CLM) version 4.5 as land-surface scheme [46]. In particular, urban areas are handled within CLM using the CLM-Urban (CLMU) module, a single-layer urban canopy model. Within CLMU the urban fraction of each grid cell is further decomposed into urban density classes—tall-building district, high-density, and medium-density areas—and the energy balance takes into account storage, roughness, radiation trapping, anthropogenic heat, and modified fluxes characteristic of urban settings.

The rest of the models - REMO2015, HadREM3-GA7-05, RACMO22E, WRF381P, WRF361H, ALADIN63 -follow a bulk urban approach. In these schemes, cities are not treated as three-dimensional structures but rather through modified bulk properties in the soil-vegetation-atmosphere transfer scheme. Surface parameters such as albedo, thermal conductivity, roughness length and displacement height are adjusted to reflect the urban context; energy balance formulations are altered to include additional urban flux components like anthropogenic heat, enhanced heat storage, and reduced evaporation [26,47]. While these bulk schemes capture general urban heat island (UHI) characteristics, particularly over typical dense city centers, they do not resolve the three-dimensional interactions and complex canopy processes (e.g., shading, multiple radiation scattering, vertical structure effects) that single-layer or multi-layer canopy models attempt to represent.

Table 1
Regional Models used in this study, with their driving GCMs.

RCM	Institution	GCM	Member	Urban config
RegCM4	ICTP	CNRM-CERFACS-CNRM-CM5	r1	UCM
		ICHEC-EC-EARTH	r12	
		MOHC-HadGEM2-ES	r1	
		MPI-M-MPI-ESM-LR	r1	
		NCC-NorESM1-M	r1	
REMO2015	GERICS	CCCma-CanESM2	r1	Bulk
		CNRM-CERFACS-CNRM-CM5	r1	
		ICHEC-EC-EARTH	r12	
		IPSL-IPSL-CM5A-MR	r1	
		MIROC-MIROC5	r1	
		MOHC-HadGEM2-ES	r1	
		MPI-M-MPI-ESM-LR	r1	
		NCC-NorESM1-M	r1	
RACMO22E	KNMI	CNRM-CERFACS-CNRM-CM5	r1	Bulk
		ICHEC-EC-EARTH	r12	
		ICHEC-EC-EARTH	r1	
		ICHEC-EC-EARTH	r3	
		IPSL-IPSL-CM5A-MR	r1	
		MOHC-HadGEM2-ES	r1	
		MPI-M-MPI-ESM-LR	r1	
		NCC-NorESM1-M	r1	
WRF381P	IPSL	CNRM-CERFACS-CNRM-CM5	r1	Bulk
		IPSL-IPSL-CM5A-MR	r1	
		ICHEC-EC-EARTH	r12	
		MOHC-HadGEM2-ES	r1	
		MPI-M-MPI-ESM-LR	r1	
		NCC-NorESM1-M	r1	
WRF361H	UHOH	ICHEC-EC-EARTH	r12	Bulk
		MOHC-HadGEM2-ES	r1	
		MPI-M-MPI-ESM-LR	r1	
ALADIN63	CNRM	CNRM-CERFACS-CNRM-CM5	r1	Bulk
		MOHC-HadGEM2-ES	r1	
		MPI-M-MPI-ESM-LR	r1	
		NCC-NorESM1-M	r1	
HadREM3	MOHC	CNRM-CERFACS-CNRM-CM5	r1	Bulk
		ICHEC-EC-EARTH	r12	
		MOHC-HadGEM2-ES	r1	
		MPI-M-MPI-ESM-LR	r1	
		NCC-NorESM1-M	r1	

4.2. City/rural outlines

To delineate urban areas and their rural surroundings within RCM outputs, we apply the algorithm developed by Diez-Sierra et al. [16] based on three static model variables: urban fraction, land area fraction, and orography, ensuring that the delineation is directly adapted to the way each model represents urban land cover and topography. Urban grid cells are identified using a minimum urban fraction threshold, in this study 40%, while rural surroundings are selected from nearby cells that meet specific criteria: urban fraction lower than 5%, sufficient land coverage (more than 70%), and similar elevation to urban cells. In the case of WRF, however, the urban fraction variable is provided as a binary mask (urban = 1, non-urban = 0) rather than a continuous fraction, and thus the thresholds of 40% for urban and 5% for rural are not applied in the same way but instead interpreted according to this categorical representation. A morphological dilation process is then iteratively applied to expand the rural mask outward from the urban core until a target rural-to-urban cell ratio is reached. This approach ensures a consistent yet flexible urban/rural classification across different cities and RCMs, and has been validated across multiple CORDEX domains [15].

Alternative methods to represent city areas in gridded climate data have been adopted in previous studies. For instance, Smid et al. [48] used the Urban Atlas produced by the European Environmental Agency to delineate greater metropolitan areas, thereby including both central municipalities and surrounding zones of urbanization, and then extracted all RCM grid cells covering these extended metropolitan extents. Their approach contrasts with earlier studies that often relied on only a single representative grid point (e.g. Guerreiro et al.,[49]), by instead incorporating the full spatial heterogeneity of each city region. However, as noted by Zhou et al. [50], administrative boundaries often differ from the actual urban extent, which may introduce inconsistencies when transferred onto model grids, since it may not align with how each RCM represents urban land cover. In contrast to coordinate- or GIS-based approaches [19,48,49], the method proposed by Diez-Sierra et al. [16] explicitly accounts for the RCM-specific representation of urban fractions and surrounding areas. This allows for a more robust, model-aware delineation of urban and rural areas, ensuring methodological consistency across multiple models and cities.

4.3. City selection

City locations are identified by using their geographic coordinates, and urban areas are then delineated based on a predefined urban threshold, and corresponding surrounding (rural) areas are defined for comparative analysis. The initial criterion for city selection was an established threshold of 40% urban fraction, which has also been applied in previous large-scale urban climate assessments [15,16]. This threshold was used to identify potential candidate cities, by locating areas containing at least one grid cell meeting the criterion. At the EUR-11 resolution (~ 12.5 km, ≈ 150 km² per grid cell), this corresponds to a minimum detectable urban footprint in the models. In addition, only cities with population exceeding 500,000 inhabitants, according to the GHS Urban Centre Database [51], were retained, to ensure that the analysis focuses on major urban areas with significant population exposure. Additionally, since we are considering seven RCMs in this study, each city was required to be classified as urban in a majority of models (approximately 60% or more), to avoid including cities that are model-dependent outliers. This multi-model consistency criterion enhances the robustness of the inter-comparison and ensures that resulting urban climate signals are not overly sensitive to the land-cover representation of any single RCM.

Finally, to ensure that the selected sample was geographically representative, we applied a spatial balancing criterion, selecting cities across the European and Northern Africa AR6 regions (NEU, WCE, MED, EEU; see Iturbide et al.[52]), with the additional aim of including both coastal and inland settings. This step is important, as coastal and inland cities may exhibit markedly distinct urban climate responses driven by variation in land-sea interactions, local circulation patterns, and surface energy balance. The final set of 40 selected cities, illustrated in Fig. 12, thus reflects both geographical diversity and the variety of urban typologies within the EURO-CORDEX domain.

4.4. Hazards Indices

Table 2 shows the list of climate hazard indices selected for this study. These indices are based on the definitions from the Expert Team on Climate Change Detection and Indices (ETCCDI;[53,54]) and have been widely used to characterize extreme temperature and precipitation events in both global and regional climate assessments ([55–58] among others). The chosen set includes temperature-based indices such as thresholds for hot days (TX35, TX30, TX25), warm nights (TN25, TN20), and heat stress conditions (Heat Index HI41, HI32). For the Heat Index, we adopt the extended formulation of Lu and Romps [59], which builds on Steadman's physiological model but removes the limitations at very hot–humid or cold–dry conditions, thereby ensuring the index is well defined for all combinations of temperature and humidity. The set further includes percentile-based indices for extreme hot days (TX90p) and warm nights (TN90p). Indicators of cold events (FD) are also included. To better capture hydrological extremes, we also include precipitation-based indices, such as consecutive dry days (CDD), number of dry days (NDD), consecutive wet days (CWD), annual maximum 1-day precipitation (RX1DAY), and extremely wet days (R99p). Finally, we add degree-day indicators (heatDD, coolDD), which provide an integrated measure of energy demand for heating and cooling.

This selection covers a broad spectrum of climate hazards relevant to urban settings, from heat stress and warm nights to droughts and extreme precipitation, enabling an integrated assessment of climate-related risks for European cities under future warming levels.

Table 2
Hazard indices used in the study

Index	Description	Input variables	Units
TN20	Tropical nights: number of days with tasmin > 20°C	tasmin	days
TN25	Equatorial nights: number of days with tasmin > 25°C	tasmin	days
TN90p	Warm nights: percentage of days when tasmin > 90th percentile of reference period (1981–2010)	tasmin	% of days
TX25	Summer days: number of days with tasmax > 25°C	tasmax	days
TX30	number of days with tasmax > 30°C	tasmax	days
TX35	number of days with tasmax > 35°C	tasmax	days
TX90p	Hot days: percentage of days when tasmax > 90th percentile of reference period (1981–2010)	tasmax	% of days
FD	Frost days: number of days with tasmin < 0°C	tasmin	days
HI41	number of days with NOAA Heat Index > 41. The 'Heat Index' is a measure of how the hot weather "feels" to the human body, when relative humidity is combined with the air temperature. The Index is computed from daily relative humidity and maximum temperature, and the annual number of days with this index above a threshold of 41°C (category: danger) is provided as HI41.	tasmax, hurs	days
HI32	number of days with NOAA Heat Index > 32	tasmax, hurs	days
heatDD	Heating degree day: Describe the need for the heating energy requirements of buildings	tas, tasmax, tasmin	degree day
coolDD	Cooling degree day: Describe the need for the cooling (air-conditioning) requirements of building, used for energy consumption	tas, tasmax, tasmin	degree day
CWD	Consecutive wet days. Maximum length of wet spell (RR ≥ 1 mm)	pr	days
CDD	Consecutive dry days: the largest number of consecutive days where daily precipitation is below a threshold of 1 mm	pr	days
NDD	Number of dry days per year. A dry day is considered when the daily precipitation is below a threshold of 1 mm	pr	days
R99p	Extremely wet days: Number of days with precipitation amount above the 99th percentile	pr	days
RX1DAY	Maximum 1 day precipitation	pr	mm

4.5 Observations

To evaluate the ability of the RCMs to represent the UHI, we use daily station data from the Global Historical Climatology Network (GHCNd [60]) and the European Climate Assessment and Dataset (ECA&D [61]). In addition, for the city of Paris, six weather stations from MétéoFrance covering the period 1980–2017 were also included. Station classification was based on the GHS-UCDB polygons delimiting urban center areas of each city. Stations located within the polygon were classified as urban, while those situated outside, but in the surrounding area, were classified as rural. To ensure consistency, elevation differences were taken into account: rural stations whose altitude differed by more than the internal elevation range of the corresponding city were excluded from the analysis. As noted by Langendijk et al. [15], these observations provide only a qualitative benchmark, since point measurements cannot be directly compared with model grid-cell averages. The analysis covers the period 1989–2008, corresponding to the evaluation run, and focuses on a subset of 12 cities for which sufficiently complete and reliable observational records were available.

Declarations

Competing interests

No competing interests to declare.

Funding

Declaration

This study was funded by the European Union's Horizon Europe Research and Innovation Actions under grant agreement No. 101081555 (IMPETUS4CHANGE). The funder had no role in the design of the study, data collection, analysis, interpretation of data, or writing of the manuscript.

Author Contribution

N. Z., E. C. and R. N. developed the conceptual approach. J. D-S and R. N. computed the urban/rural masks. N. Z. and F. R. conducted the computation of the Hazard Indices. G. G. provided software development for the Heat Index computation. N. Z. conducted the urban heat island analysis and took the lead on writing the manuscript. All authors have substantially contributed to writing and revising the manuscript.

Acknowledgement

We acknowledge the support from the European Union's HORIZON Research and Innovation Actions under grant agreement No 101081555, project IMPETUS4CHANGE. G.S.L.

Data Availability

EURO-CORDEX data for daily maximum and minimum near surface temperature, relative humidity, orography, and land area fraction are publicly available through ESGF ([https://esgf-data.dkrz.de/search/cordex-dkrz/](https:/esgf-data.dkrz.de/search/cordex-dkrz)).Urban surface area fractions were collected and post-processed as part of this work and will be publicly available together with this publication.

References

1. World Bank Open Data. World Bank Open Data https://data.worldbank.org.
2. Intergovernmental Panel On Climate Change (Ipcc). Climate Change 2022 – Impacts, Adaptation and Vulnerability: Working Group II Contribution to the Sixth Assessment Report of the Intergovernmental Panel on Climate Change. (Cambridge University Press, 2023). doi:10.1017/9781009325844.
3. Intergovernmental Panel On Climate Change (Ipcc). Climate Change 2021 – The Physical Science Basis: Working Group I Contribution to the Sixth Assessment Report of the Intergovernmental Panel on Climate Change. (Cambridge University Press, 2023). doi:10.1017/9781009157896.
4. Copernicus Climate Change Service (C3S). European State of the Climate 2024. https://climate.copernicus.eu/esotc/2024 (2025) doi:10.24381/14J9-S541.
5. Knutzen, F. *et al.* Impacts on and damage to European forests from the 2018–2022 heat and drought events. *Nat. Hazards Earth Syst. Sci.* 25, 77–117 (2025).
6. Felsche, E., Böhnisch, A., Poschlod, B. & Ludwig, R. European hot and dry summers are projected to become more frequent and expand northwards. *Commun. Earth Environ.* 5, 410 (2024).
7. Driessen, P. P. *et al.* Governance strategies for improving flood resilience in the face of climate change. *Water* 10, 1595 (2018).
8. Kusaka, H., Hara, M. & Takane, Y. Urban climate projection by the WRF model at 3-km horizontal grid increment: dynamical downscaling and predicting heat stress in the 2070's August for Tokyo, Osaka, and Nagoya metropolises. *J. Meteorol. Soc. Jpn.* 90, 47–63 (2012).
9. Argüeso, D., Di Luca, A. & Evans, J. P. Precipitation over urban areas in the western Maritime Continent using a convection-permitting model. *Clim. Dyn.* 47, 1143–1159 (2016).
10. Krayenhoff, E. S., Moustaoui, M., Broadbent, A. M., Gupta, V. & Georgescu, M. Diurnal interaction between urban expansion, climate change and adaptation in US cities. *Nat. Clim. Change* 8, 1097–1103 (2018).
11. Langendijk, G. S., Rechid, D., Sieck, K. & Jacob, D. Added value of convection-permitting simulations for understanding future urban humidity extremes: case studies for Berlin and its surroundings. *Weather Clim. Extrem.* 33, 100367 (2021).
12. Michau, Y. *et al.* Projected evolution of the Urban climate and heatwaves using an ensemble of convection-permitting regional climate models. *Clim. Change* 178, 154 (2025).
13. Huszar, P. *et al.* Regional climate model assessment of the urban land-surface forcing over central Europe. *Atmospheric Chem. Phys.* 14, 12393–12413 (2014).
14. Daniel, M. *et al.* Benefits of explicit urban parameterization in regional climate modeling to study climate and city interactions. *Clim. Dyn.* 52, 2745–2764 (2019).
15. Langendijk, G. S. et al. Representation of global mega-cities and their urban heat island in CORDEX-CORE regional climate model simulations. Npj Urban Sustain.
16. Diez Sierra, J., J. et al. A global CORDEX-based dataset delineating urban areas and their surroundings to assess climate change on megacities. Sci. Data.
17. Shu, C. *et al.* Added value of convection permitting climate modelling in urban overheating assessments. *Build. Environ.* 207, 108415 (2022).
18. Pei, L., Miao, S.-G., Huang, X.-Y., Yan, Z.-W. & Chen, D. Assessing the added value of convection-permitting modeling for urban climate research: A case study in eastern China. *Adv. Clim. Change Res.* 16, 1–11 (2025).
19. Schwingshackl, C., Daloz, A. S., Iles, C., Aunan, K. & Sillmann, J. High-resolution projections of ambient heat for major European cities using different heat metrics. *Nat. Hazards Earth Syst. Sci.* 24, 331–354 (2024).
20. Mărmureanu, L., Antonescu, B., Ene, D., Andrei, S. & Turcu, R. Changes in the thermal stress across Europe between 1940–2023. *Int. J. Biometeorol.* 69, 3569–3586 (2025).

21. Kusaka, H. & Kimura, F. Thermal effects of urban canyon structure on the nocturnal heat island: Numerical experiment using a mesoscale model coupled with an urban canopy model. *J. Appl. Meteorol.* 43, 1899–1910 (2004).
22. Lazzarini, M., Molini, A., Marpu, P. R., Ouarda, T. B. M. J. & Ghedira, H. Urban climate modifications in hot desert cities: The role of land cover, local climate, and seasonality. *Geophys. Res. Lett.* 42, 9980–9989 (2015).
23. Blackport, R., Sigmond, M. & Screen, J. A. Models and observations agree on fewer and milder midlatitude cold extremes even over recent decades of rapid Arctic warming. *Sci. Adv.* 10, eadp1346 (2024).
24. Ruosteenoja, K. & Jylhä, K. Extreme Cold Days and Spells in Northern Europe at 0.5°C–2.0°C Global Warming Levels. *Int. J. Climatol.* 45, e8875 (2025).
25. Salamanca, F. *et al.* Assessing summertime urban air conditioning consumption in a semiarid environment. *Environ. Res. Lett.* 8, 034022 (2013).
26. Hamdi, R. *et al.* The State-of-the-Art of Urban Climate Change Modeling and Observations. *Earth Syst. Environ.* 4, 631–646 (2020).
27. Demuzere, M. *et al.* A global map of Local Climate Zones to support earth system modelling and urban scale environmental science. *Earth Syst. Sci. Data Discuss.* 2022, 1–57 (2022).
28. CORDEX. CORDEX experiment design for dynamical downscaling of CMIP6. https://cordex.org/wp-content/uploads/2021/05/CORDEX-CMIP6_exp_design_RCM.pdf (2021).
29. Karlický, J. *et al.* Multi-model comparison of urban heat island modelling approaches. *Atmospheric Chem. Phys.* 18, 10655–10674 (2018).
30. SITES, M. O. A. U. Initial Guidance To Obtain Representative Meteorological Observations At Urban Sites. https://www.researchgate.net/profile/T-Oke/publication/265347633_Initial_guidance_to_obtain_representative_meteorological_observations_at_urban_sites/links/567a3b4d08ae361c2f681d5b guidance-to-obtain-representative-meteorological-observations-at-urban-sites.pdf (2025).
31. Stewart, I. D. & Oke, T. R. Local Climate Zones for Urban Temperature Studies. *Bull. Am. Meteorol. Soc.* 93, 1879–1900 (2012).
32. Gaffin, S. R. *et al.* Variations in New York city's urban heat island strength over time and space. *Theor. Appl. Climatol.* 94, 1–11 (2008).
33. Lehnert, M., Janků, Z., Novotný, D., Jurek, M. & Geletič, J. Assessment of air temperature indices and urban heat island intensity based on two meteorological networks in Prague, Czechia. *Theor. Appl. Climatol.* 156, 470 (2025).
34. Arnds, D., Böhner, J. & Bechtel, B. Spatio-temporal variance and meteorological drivers of the urban heat island in a European city. *Theor. Appl. Climatol.* 128, 43–61 (2017).
35. Koomen, E. & Diogo, V. Assessing potential future urban heat island patterns following climate scenarios, socio-economic developments and spatial planning strategies. *Mitig. Adapt. Strateg. Glob. Change* 22, 287–306 (2017).
36. Li, Y., Schubert, S., Kropp, J. P. & Rybski, D. On the influence of density and morphology on the Urban Heat Island intensity. *Nat. Commun.* 11, 2647 (2020).
37. Spinoni, J., Vogt, J. V., Naumann, G., Barbosa, P. & Dosio, A. Will drought events become more frequent and severe in Europe? *Int. J. Climatol.* 38, 1718–1736 (2018).
38. Jacob, D. *et al.* EURO-CORDEX: new high-resolution climate change projections for European impact research. *Reg. Environ. Change* 14, 563–578 (2014).
39. Giorgi, F. & Gutowski, W. J. Regional Dynamical Downscaling and the CORDEX Initiative. *Annu. Rev. Environ. Resour.* 40, 467–490 (2015).
40. Taylor, K. E., Stouffer, R. J. & Meehl, G. A. An Overview of CMIP5 and the Experiment Design. *Bull. Am. Meteorol. Soc.* 93, 485–498 (2012).
41. Diez-Sierra, J. *et al.* The Worldwide C3S CORDEX Grand Ensemble: A Major Contribution to Assess Regional Climate Change in the IPCC AR6 Atlas. *Bull. Am. Meteorol. Soc.* 103, E2804–E2826 (2022).
42. Ciarlo`, J. M. *et al.* A new spatially distributed added value index for regional climate models: the EURO-CORDEX and the CORDEX-CORE highest resolution ensembles. *Clim. Dyn.* 57, 1403–1424 (2021).
43. Lin, C., Kjellström, E., Wilcke, R. A. I. & Chen, D. Present and future European heat wave magnitudes: climatologies, trends, and their associated uncertainties in GCM-RCM model chains. *Earth Syst. Dyn.* 13, 1197–1214 (2022).
44. Dee, D. P. *et al.* The ERA-Interim reanalysis: configuration and performance of the data assimilation system. *Q. J. R. Meteorol. Soc.* 137, 553–597 (2011).
45. Van Vuuren, D. P. *et al.* The representative concentration pathways: an overview. *Clim. Change* 109, 5–31 (2011).
46. Oleson, K. W. *et al.* Technical description of version 4.5 of the Community Land Model (CLM). *Tech. Descr. Version 45 Community Land Model CLM2013 NCARTN-503 STR* 503, (2013).
47. Kusaka, H., Kondo, H., Kikegawa, Y. & Kimura, F. A Simple Single-Layer Urban Canopy Model For Atmospheric Models: Comparison With Multi-Layer And Slab Models. *Bound.-Layer Meteorol.* 101, 329–358 (2001).
48. Smid, M., Russo, S., Costa, A. C., Granell, C. & Pebesma, E. Ranking European capitals by exposure to heat waves and cold waves. *Urban Clim.* 27, 388–402 (2019).
49. Guerreiro, S. B., Dawson, R. J., Kilsby, C., Lewis, E. & Ford, A. Future heat-waves, droughts and floods in 571 European cities. *Environ. Res. Lett.* 13, 034009 (2018).
50. Zhou, B., Rybski, D. & Kropp, J. P. On the statistics of urban heat island intensity. *Geophys. Res. Lett.* 40, 5486–5491 (2013).
51. Pesaresi, M. *et al.* Advances on the Global Human Settlement Layer by joint assessment of Earth Observation and population survey data. *Int. J. Digit. Earth* 17, 2390454 (2024).
52. Iturbide, M. *et al.* An update of IPCC climate reference regions for subcontinental analysis of climate model data: definition and aggregated datasets. *Earth Syst. Sci. Data* 12, 2959–2970 (2020).
53. Data, C. Guidelines on analysis of extremes in a changing climate in support of informed decisions for adaptation. *World Meteorol. Organ.* 1500, 72 (2009).

54. Zhang, X. *et al.* Indices for monitoring changes in extremes based on daily temperature and precipitation data. *WIREs Clim. Change* 2, 851–870 (2011).
55. Sillmann, J., Kharin, V. V., Zhang, X., Zwiers, F. W. & Bronaugh, D. Climate extremes indices in the CMIP5 multimodel ensemble: Part 1. Model evaluation in the present climate. *J. Geophys. Res. Atmospheres* 118, 1716–1733 (2013).
56. Rusticucci, M. & Zazulie, N. Attribution and projections of temperature extreme trends in South America based on CMIP5 models. *Ann. N. Y. Acad. Sci.* 1504, 154–166 (2021).
57. Guan, J., Yao, J., Li, M., Li, D. & Zheng, J. Historical changes and projected trends of extreme climate events in Xinjiang, China. *Clim. Dyn.* 59, 1753–1774 (2022).
58. Ossó, A., Allan, R. P., Hawkins, E., Shaffrey, L. & Maraun, D. Emerging new climate extremes over Europe. *Clim. Dyn.* 58, 487–501 (2022).
59. Lu, Y.-C. & Romps, D. M. Extending the Heat Index. *J. Appl. Meteorol. Climatol.* 61, 1367–1383 (2022).
60. Menne, M. J., Durre, I., Vose, R. S., Gleason, B. E. & Houston, T. G. An Overview of the Global Historical Climatology Network-Daily Database. *J. Atmospheric Ocean. Technol.* 29, 897–910 (2012).
61. Klein Tank, A. M. G. *et al.* Daily dataset of 20th-century surface air temperature and precipitation series for the European Climate Assessment. *Int. J. Climatol.* 22, 1441–1453 (2002).

Figures

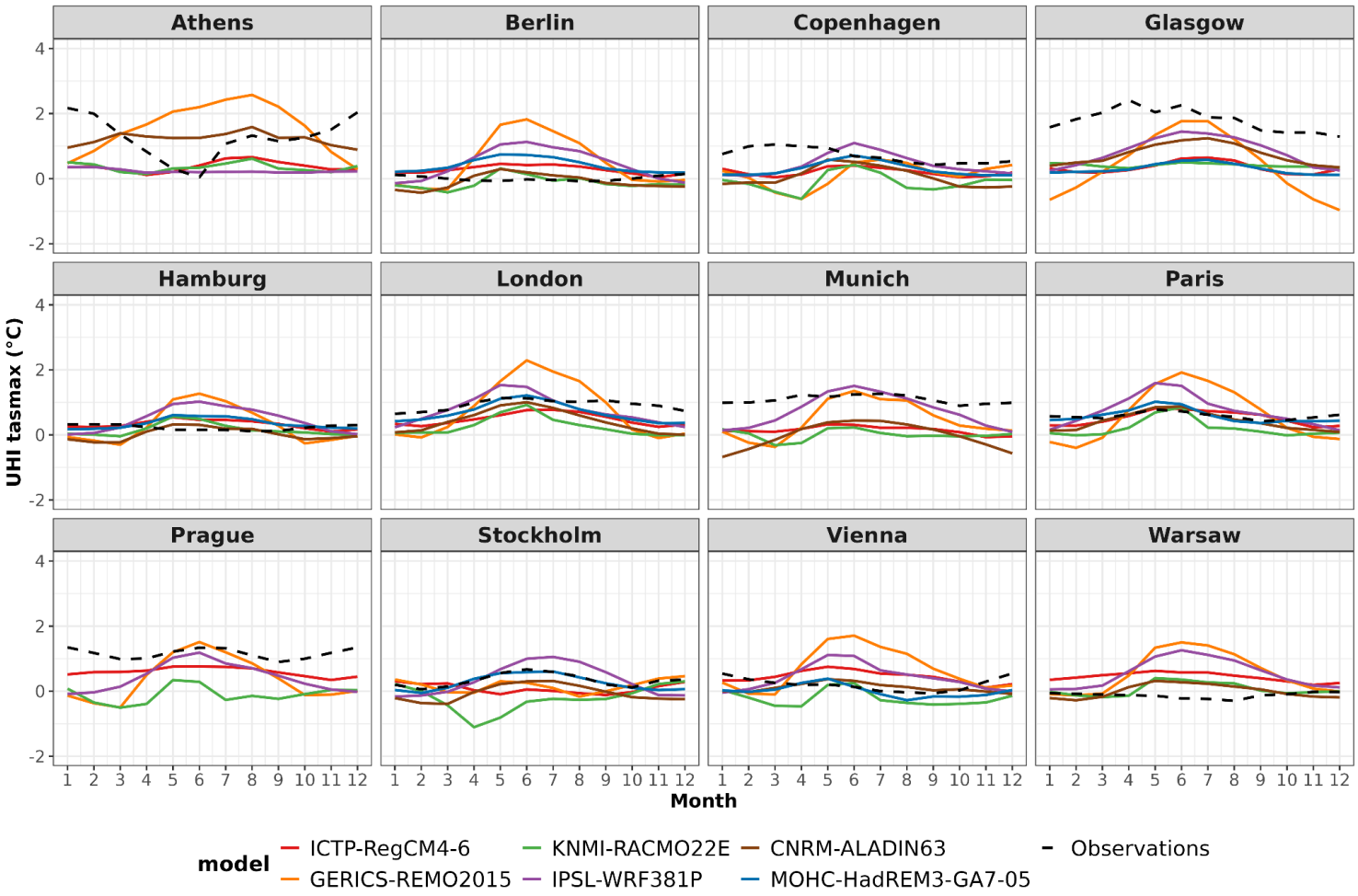


Figure 1

Annual cycle of UHI of tasmax for the evaluation runs and the observations for the period 1989-2008.

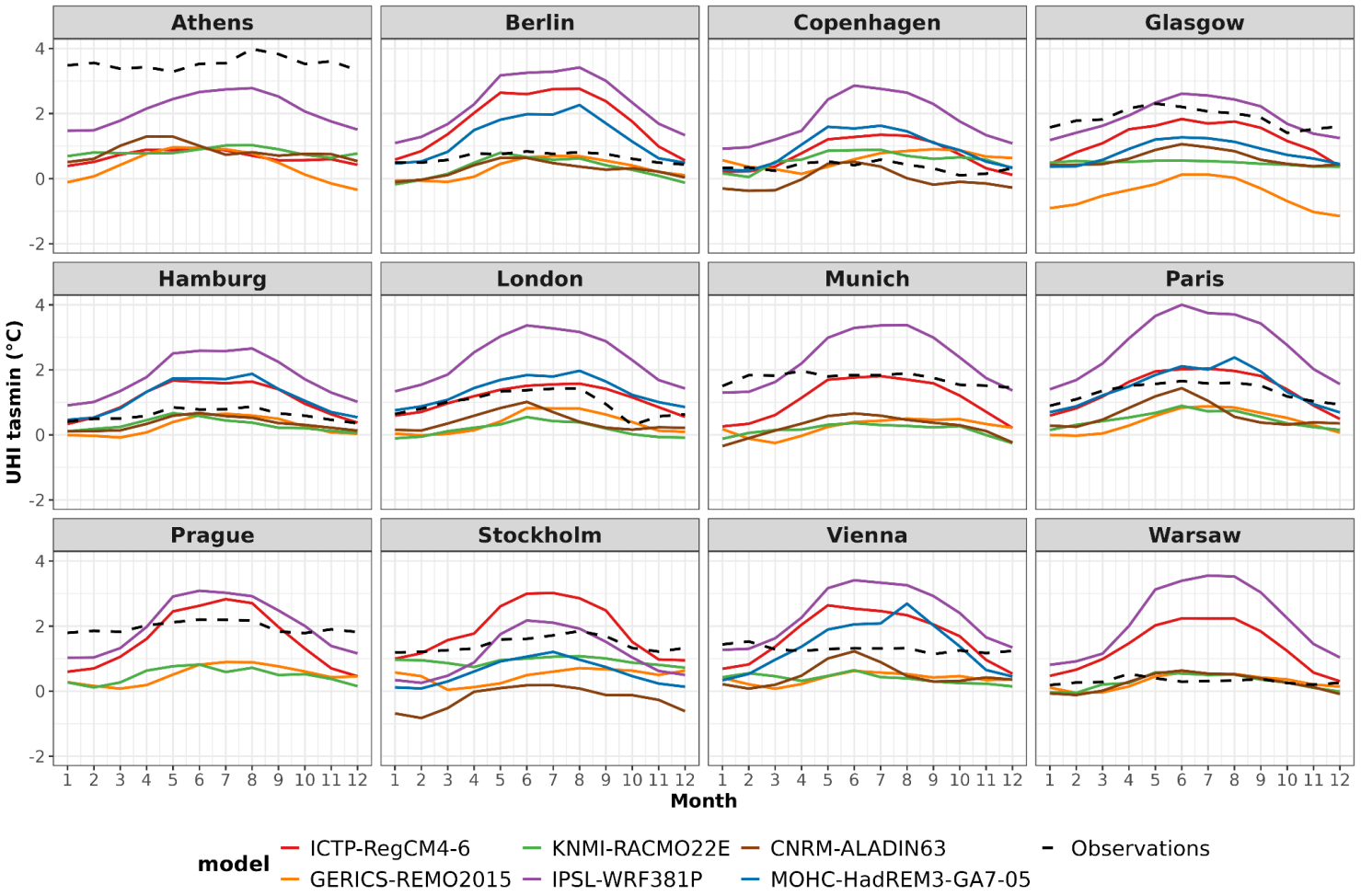


Figure 2

Annual cycle of UHI of tasmin for the evaluation runs and the observations for the period 1989-2008.

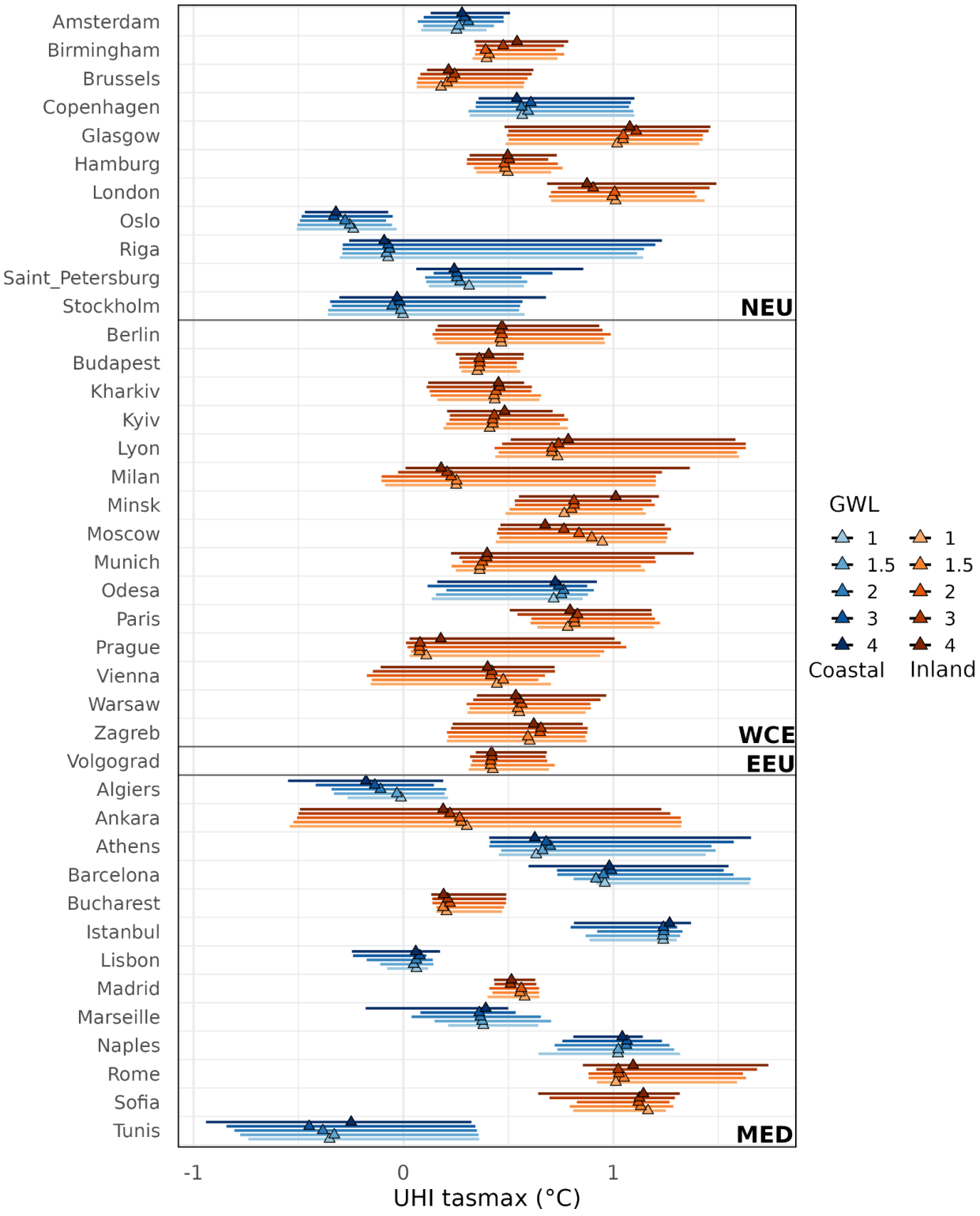


Figure 3

Projected Urban Heat Island (UHI) of tasmax for each city at 1.0, 1.5, 2.0, 3.0, and 4.0 global warming levels (GWLs) under RCP8.5. Triangles indicate the ensemble median, and horizontal lines represent the 25th–75th percentile range. Blue tones denote coastal cities, orange tones inland cities. Cities are grouped by AR6 regions (NEU, WCE, EEU, MED).

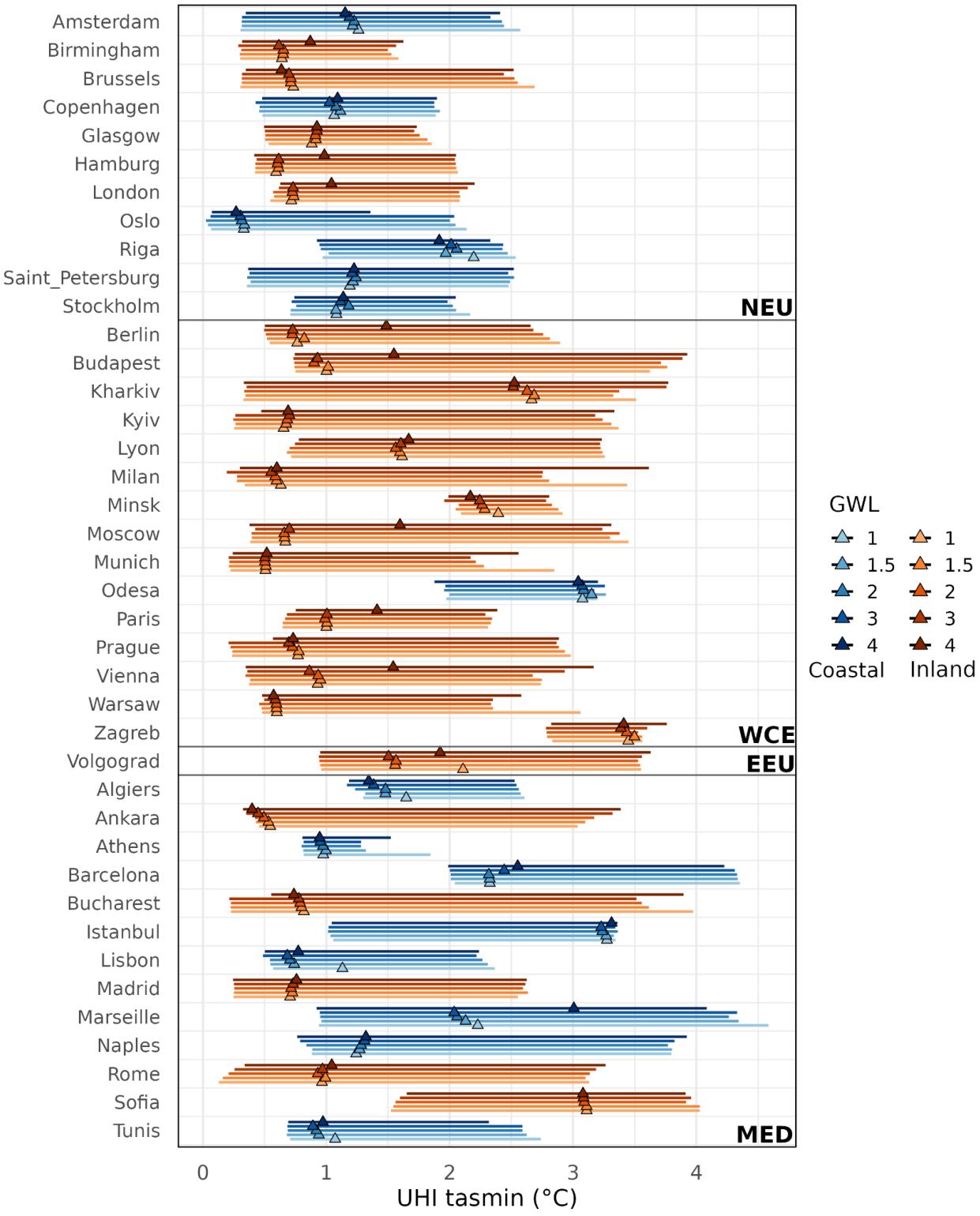


Figure 4

Same as Figure 3 but for tasmin.

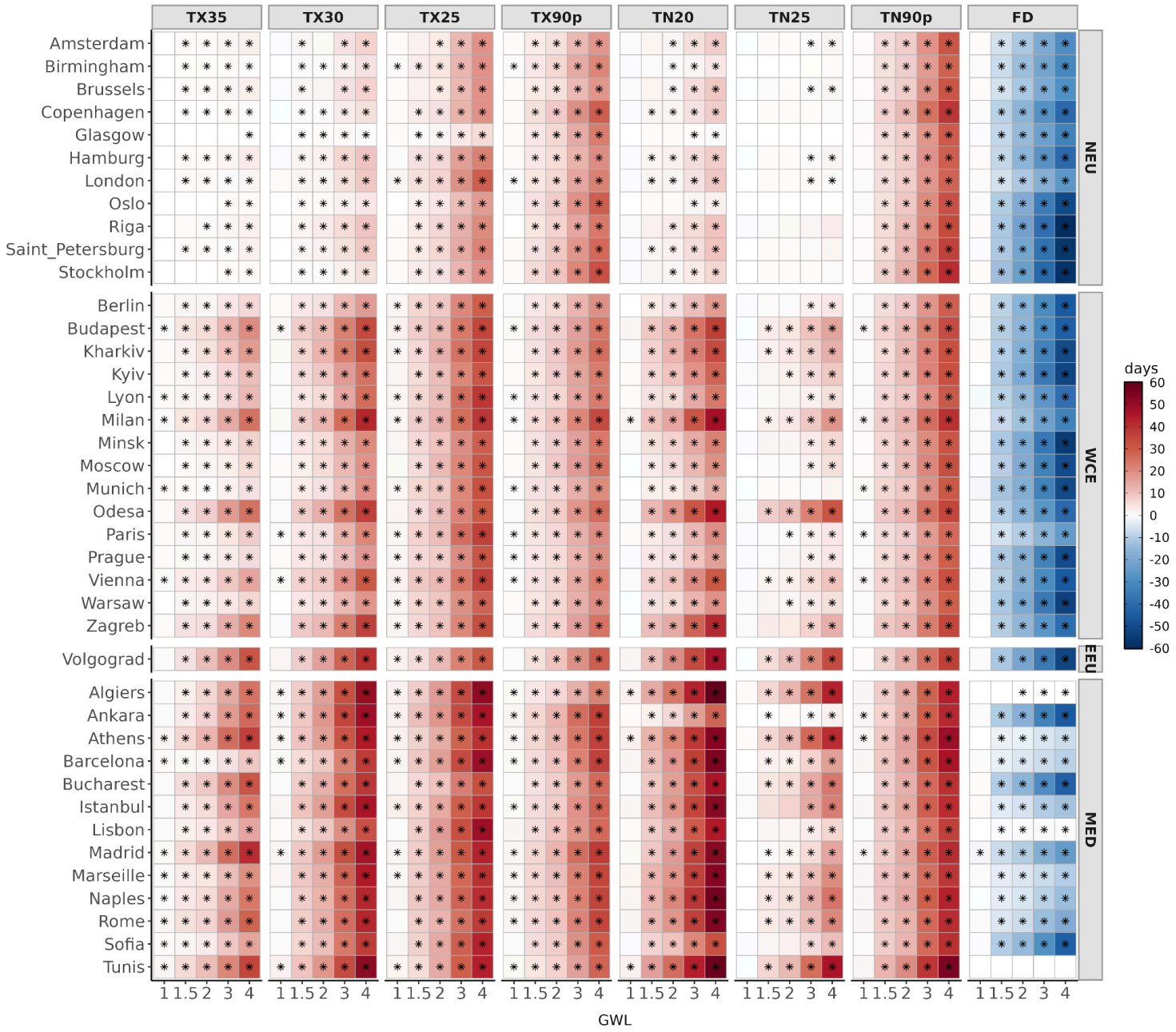


Figure 5

Heat map of index changes (day/year) with respect to the reference period (1995-2014) for each city at the 5 different Global Warming Levels (1.0, 1.5, 2.0, 3.0, 4.0) for temperature-based indices. Asterisks indicate significant changes at 95% confidence level with a t-student's test.

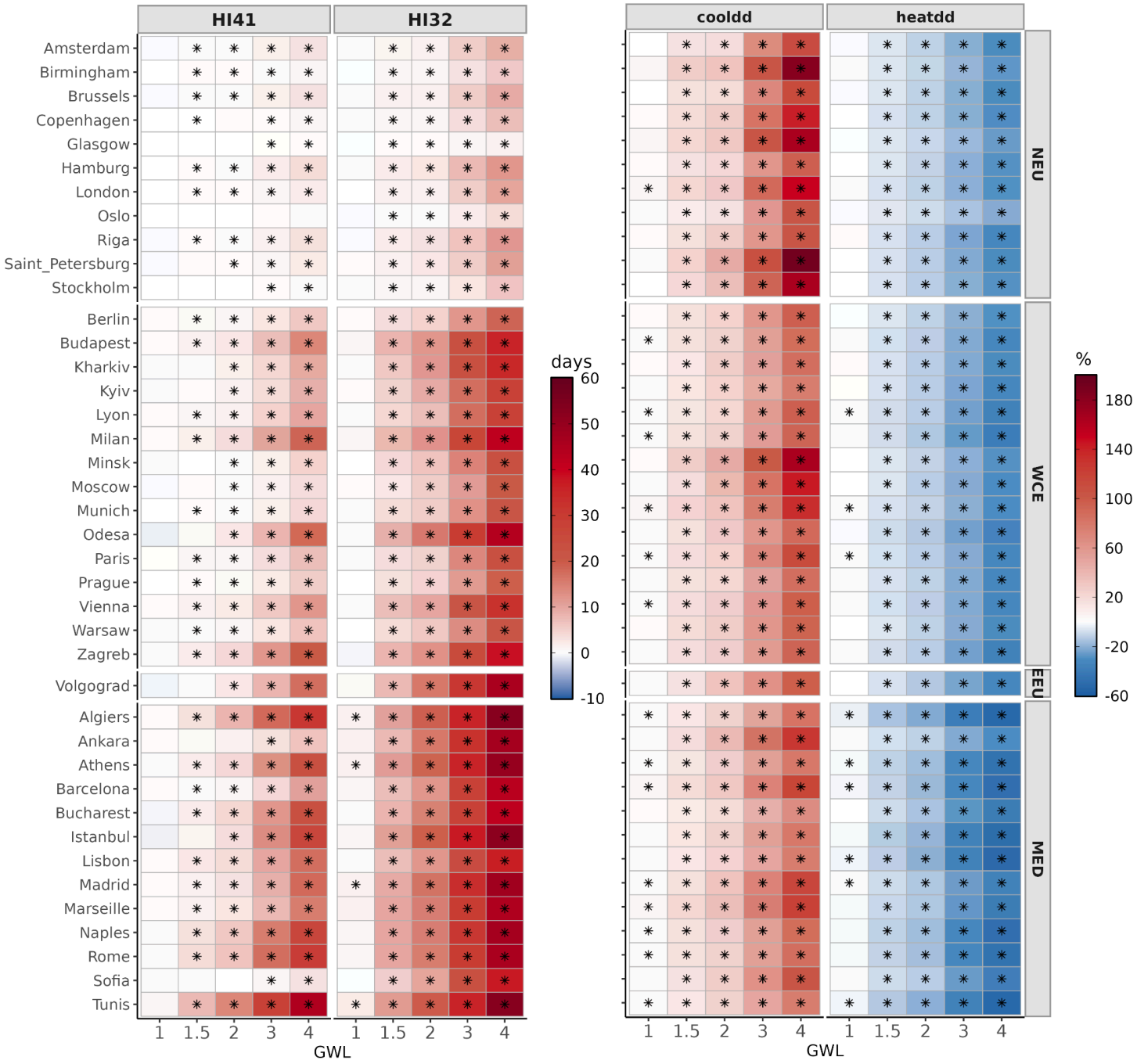


Figure 6

Heat map of the percentage change with respect to the reference period (1995–2014) for impact-oriented indices (HI41, HI32, coolDD, heatDD) for each city at five Global Warming Levels (1.0, 1.5, 2.0, 3.0, 4.0). Asterisks denote statistically significant changes at the 95% confidence level based on a Student's t-test.

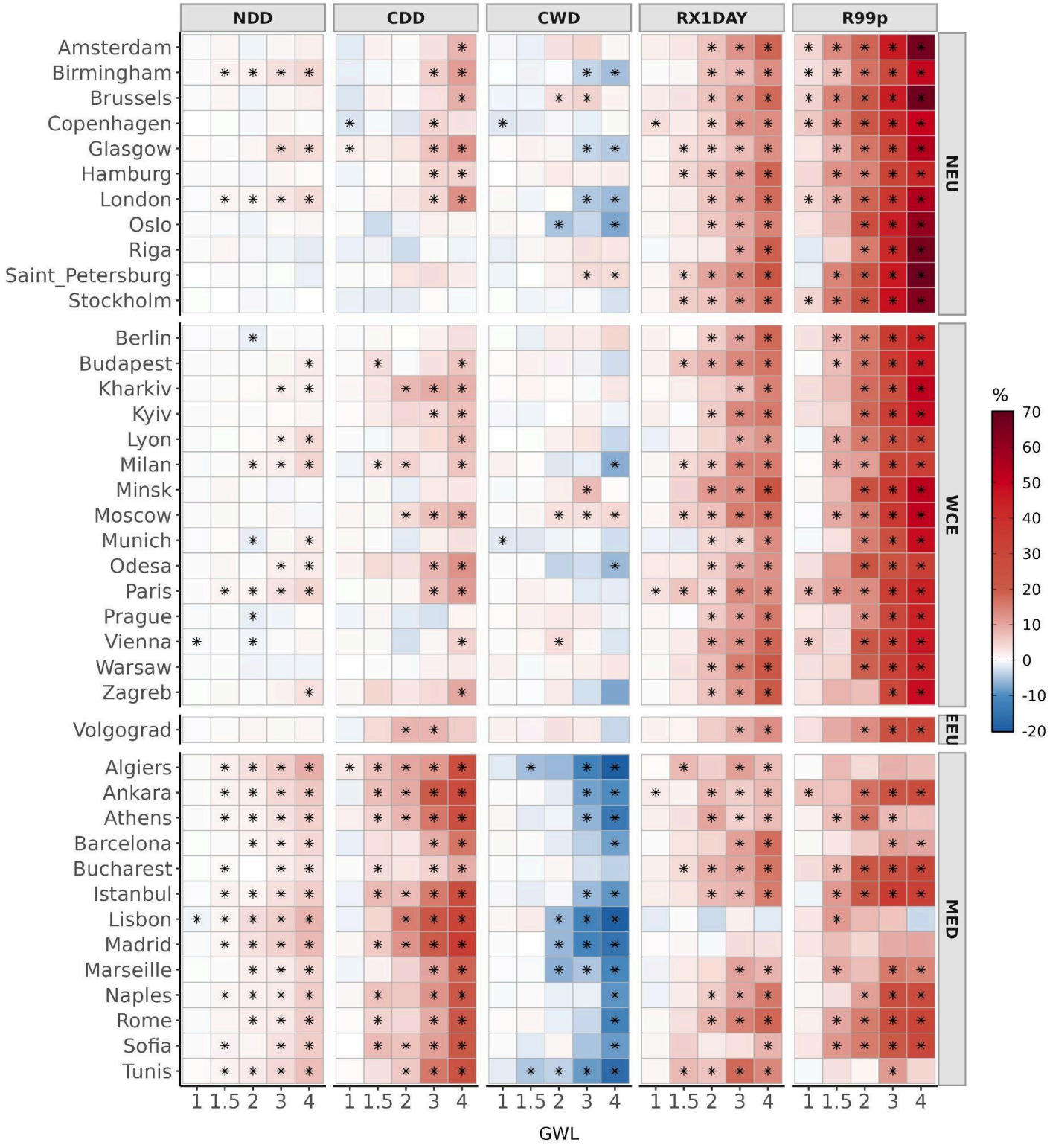


Figure 7

Heat map of the percentage change with respect to the reference period (1995–2014) for precipitation-based indices (NDD, CDD, CWD, RX1DAY, R99p)for each city at each of the five Global Warming Levels (1.0, 1.5, 2.0, 3.0, 4.0). Asterisks denote statistically significant changes at the 95% confidence level based on a Student's t-test.

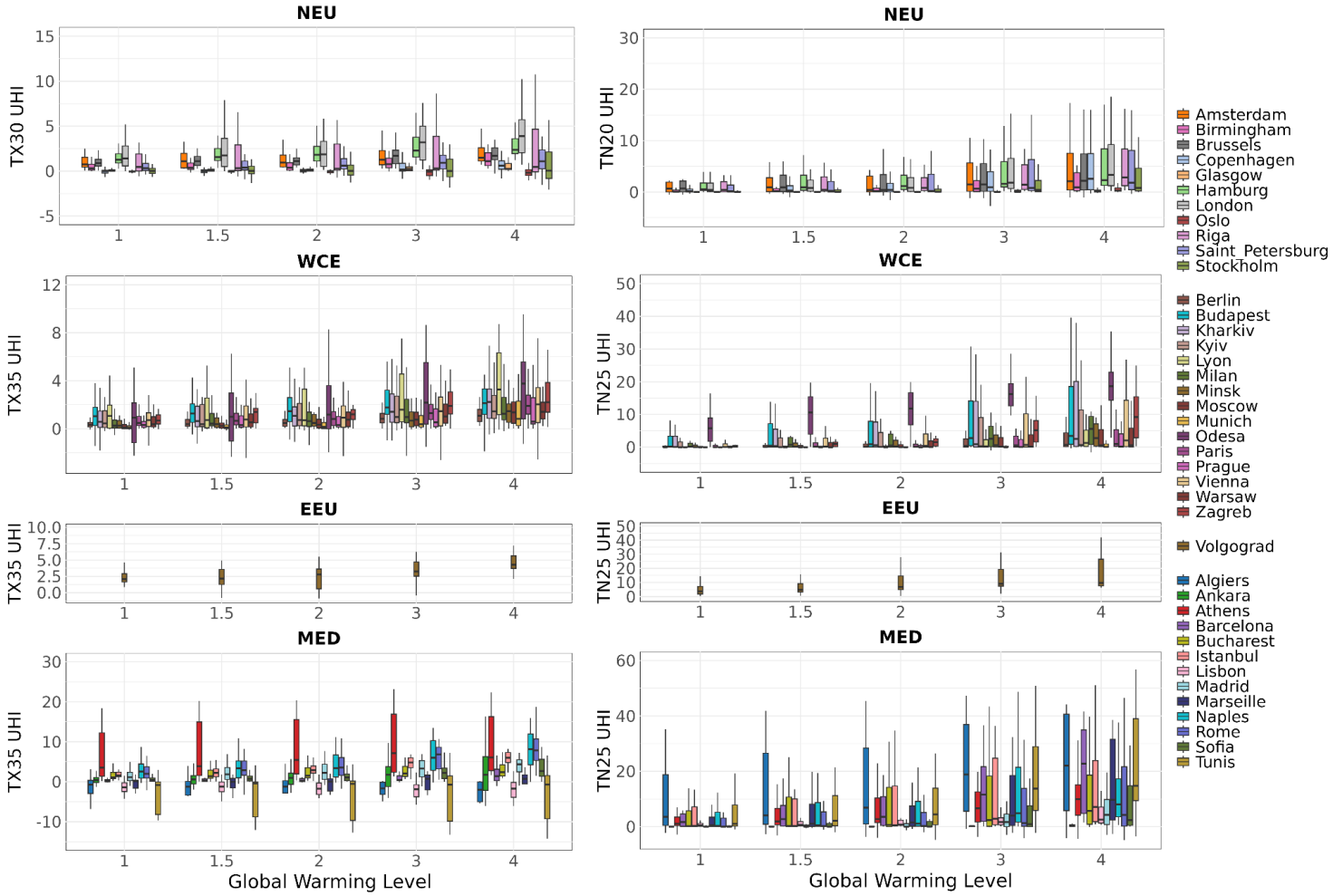


Figure 8

Boxplot of UHI for tasmax (left) and tasmin (right) threshold indices for cities grouped by region for each GWL. TX30 (left) and TN20 (right) for NEU region, and TX35 (left) and TN25 (right) for WCE, EEU and MED regions. Size of the box indicates the range of the 25th–75th percentile range, horizontal line indicates the median of all members.

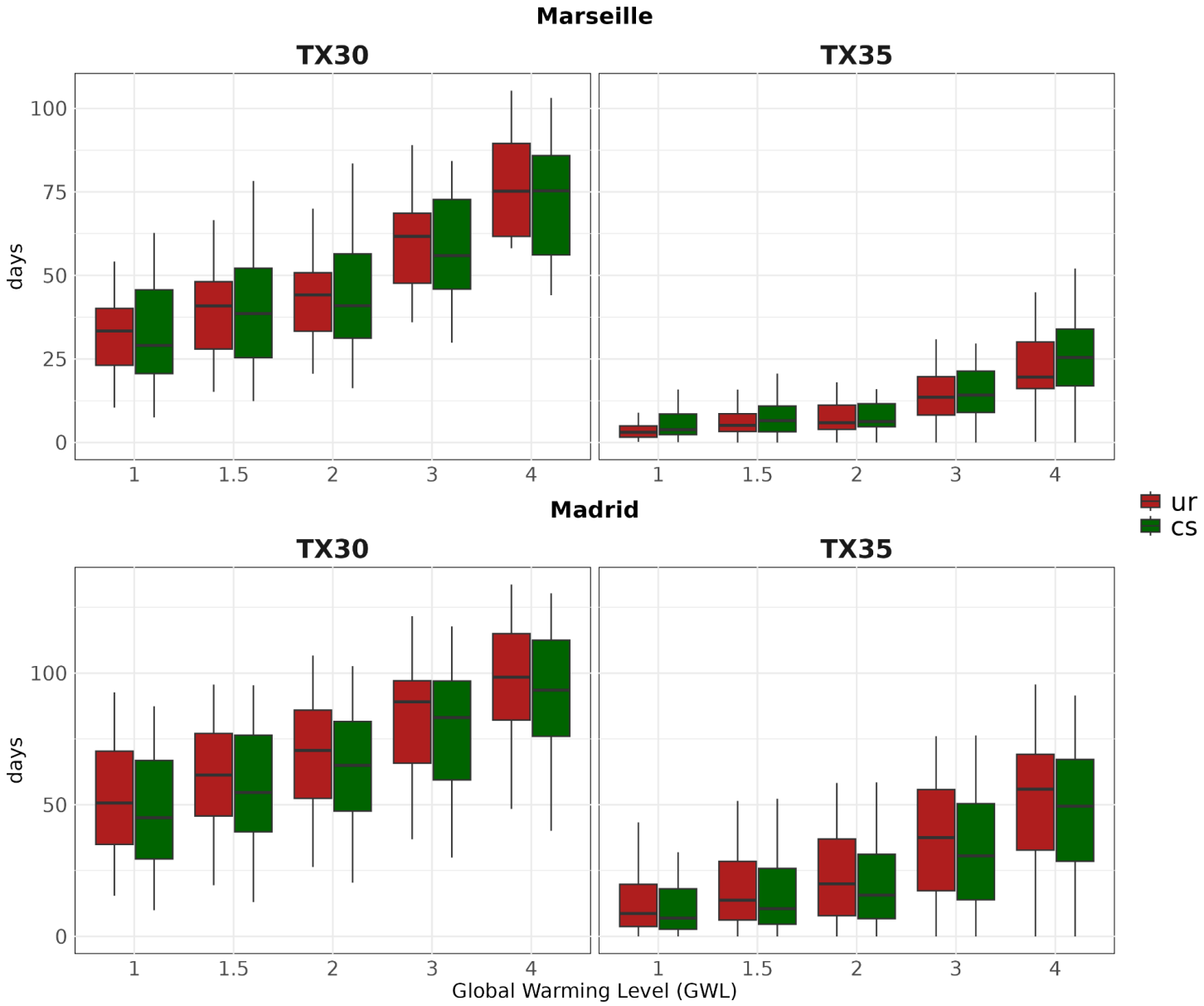


Figure 9

Boxplots of TX30 (left) and TX35 (right) for the 1.0, 1.5, 2.0, 3.0 and 4.0 GWLs for the coastal city of Marseille (upper panel) and the inland city of Madrid (lower panel). Urban areas in red and countryside in green.

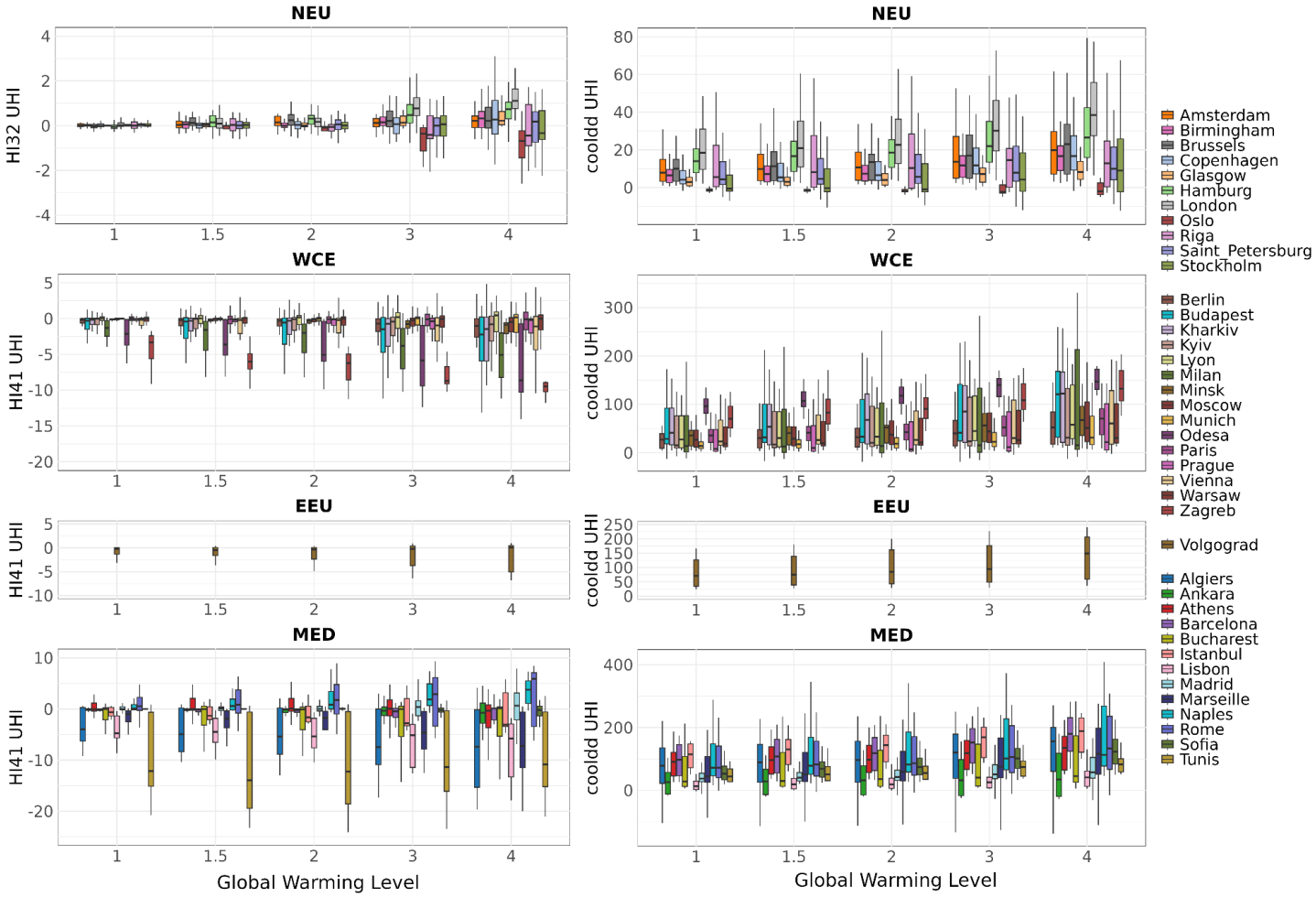


Figure 10

Same as Figure 8 but for HI32 in NEU and HI41 in WCE, EEU and MED (left) and coolDD (right) indices.

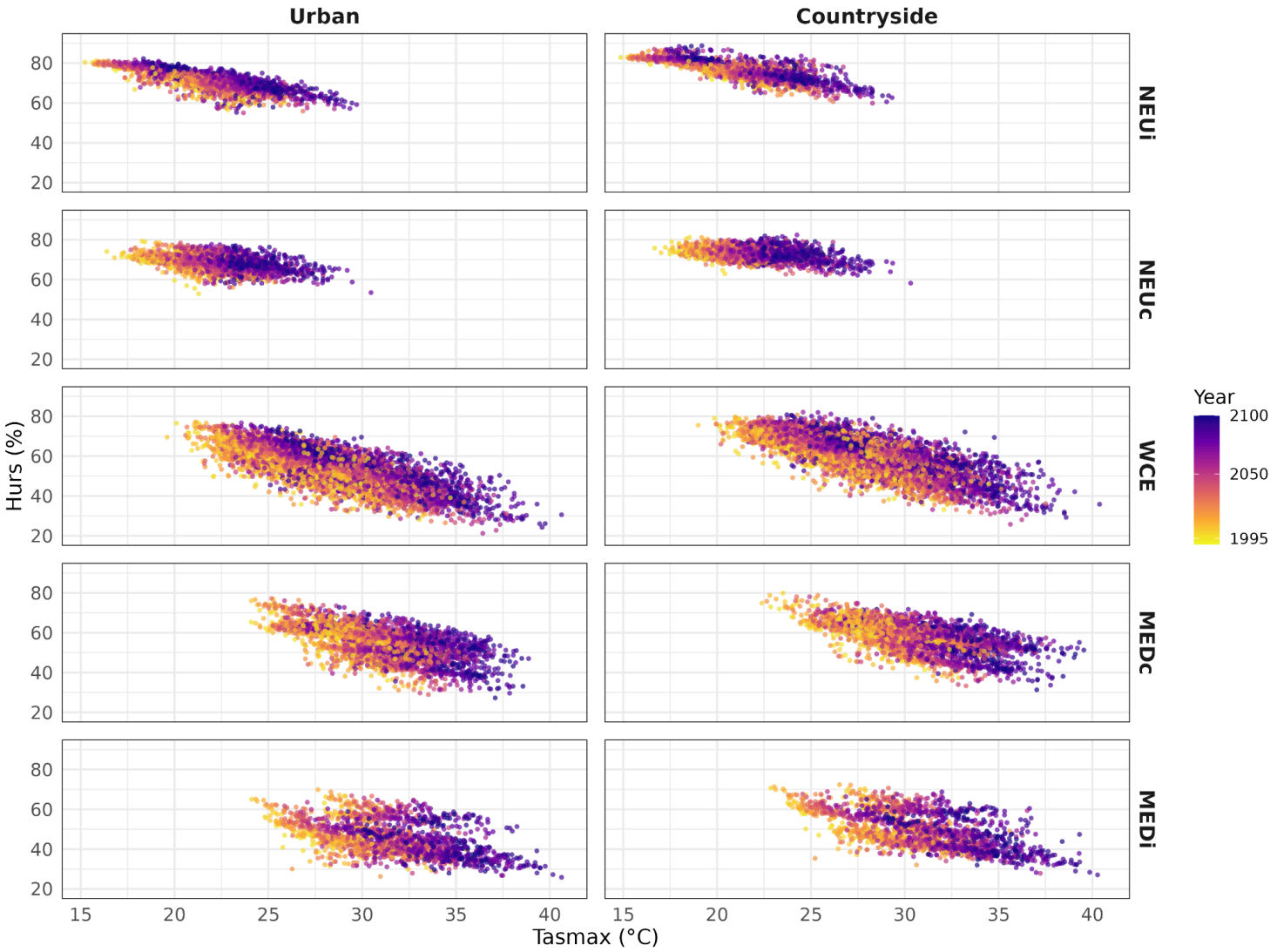


Figure 11

Relative humidity (hurs) vs Maximum temperature (tasmax) for all cities in each region. The NEU and MED regions are split into coastal cities (c) and inland cities (i). Individual points represent the multimodel summer (JJA) mean and the color scale indicates the year in the period 1995-2100.

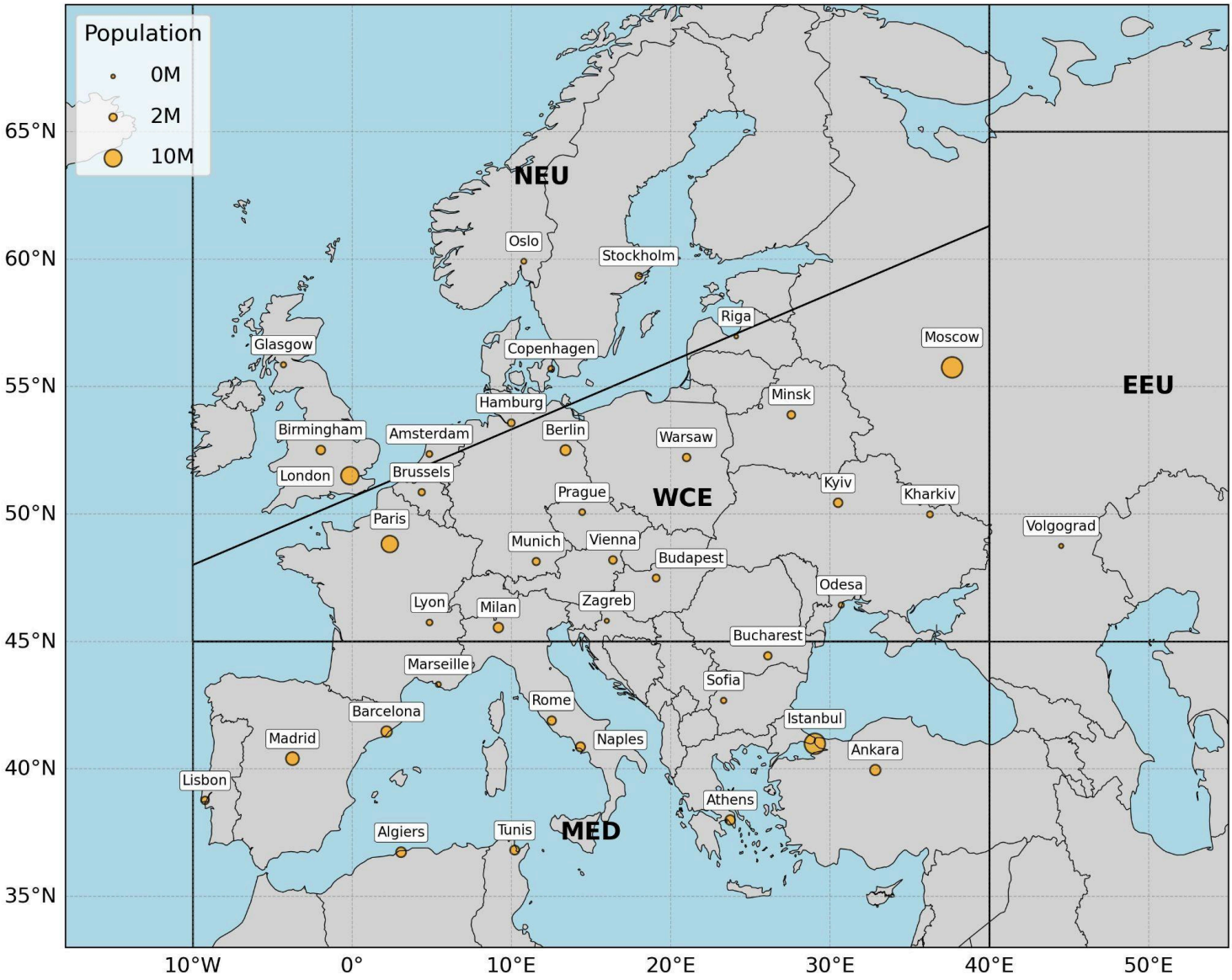


Figure 12

Location of selected cities and the AR6 regions. Size of the dots represent the population from the GHS-UCDB database.